TUJNAS

Original Article

Thamar University Journal of Natural & Applied Sciences 10(1) (2025) 16– 24

DOI: https://doi.org/10.59167/tujnas.v10i1.2675

Design and Photocatalytic Evaluation of CdO–ZnO–Co_3O_4 Ternary Nanocomposite Synthesized by Co-precipitation Method

A.M. Abdulwahab[1,*], Thana Shuga Aldeen[2,], Shadha Nasser Aziz[2,3], and Abdullah Ahmed Ali Ahmed[1,4]**

[1]Physics Department, Faculty of Applied Science, Thamar University, Dhamar 87246, Yemen

[2]Physics Department, Faculty of Science, Sana'a University, Sana'a, Yemen

[3]Al-Darb Community College, Dhamar, Yemen

[4]Center for Hybrid Nanostructures (CHyN) and Fachbereich Physik, Universität Hamburg, 20146 Hamburg, Germany

Corresponding Authors:
*A.M. Abdulwahab, Physics Department, Faculty of Applied Science, Thamar University, Dhamar 87246, Yemen. E-mail address: abduhabdulwahab@yahoo.com
**Thana Shuga Aldeen, Physics Department, Faculty of Science, Sana'a University, Sana'a, Yemen. E-mail address: thana.sh.aldeen@gmail.com

Received: 6 May 2025. Received (in revised form): 25 May 2025. Accepted: 29 May 2025. Published: 28 June 2025.

Abstract

A CdO–ZnO–Co_3O_4 ternary nanocomposite was synthesized via the co-precipitation method. Transmission electron microscopy (TEM) confirmed the spherical morphology of the nanoparticles, with average particle sizes of 60.8 nm (CdO), 51.8 nm (ZnO), 33.3 nm (Co_3O_4), and a significantly reduced size of 13.82 nm for the nanocomposite. Crystallographic analysis revealed cubic structures for CdO and Co_3O_4, and a hexagonal structure for ZnO. Elemental composition was validated through total reflection X-ray fluorescence (TXRF). Diffuse reflectance spectroscopy (DRS) was employed to assess the optical properties, including reflectance and band gap energies. CdO and ZnO exhibited direct band gaps of 2.0 eV and 3.15 eV, respectively, whereas Co_3O_4 presented two band gap transitions at 1.0 eV and 1.43 eV, corresponding to charge transfers from O^{2-} to Co^{3+} and Co^{2+} ions. The ternary nanocomposite demonstrated a narrowed band gap of 1.4 eV. Photocatalytic testing against methylene red (MR) dye under UV irradiation showed a notable degradation efficiency of 33.5% within 30 minutes. These results suggest that the CdO–ZnO–Co_3O_4 nanocomposite holds strong potential for application in wastewater treatment.

Keywords: XRD; TXRF; Band gap energy; Photocatalyst; CdO-ZnO-Co_3O_4 Nanocomposite.

1. Introduction

Photolysis refers to the chemical decomposition of a molecule triggered by the absorption of light energy. In the context of nanocomposites, photolysis plays a vital role in understanding both the degradation of the polymer matrix and the light-induced release of embedded nanoparticles. This phenomenon is particularly significant for nanocomposites containing semiconductor particles like TiO_2, CeO_2, or ZnO, which exhibit photocatalytic behavior under light exposure. Such materials find applications in self-cleaning coatings, environmental remediation, and water purification. Researchers have explored a variety of parameters that influence photodegradation, including polymer type, nanofiller content, and light wavelength. Of particular concern is the release potential of nanoparticles from polymer matrices under illumination, which carries both functional and environmental implications [1].

Transition metal oxides (TMOs) have garnered extensive research interest due to their tunable synthesis pathways and ability to form multiple crystalline phases with varied metal-to-oxygen ratios. These structural variations impact their physical properties and broaden their application range [2,3]. Metal oxide-based nanocomposites are now widely studied for their roles in energy-related technologies, including solar cells, gas sensors, UV detectors, fuel cells, and batteries [4,5].

Cadmium oxide (CdO) is a well-known n-type semiconductor with a direct band gap in the range of 2.2–2.5 eV. Its notable features—such as low electrical resistivity and high transparency in the visible spectrum—make it a strong candidate for various optoelectronic and catalytic applications. These include solar energy devices, gas sensing, UV absorption, and catalytic oxidation [6].

Zinc oxide (ZnO), another widely used n-type semiconductor, has been extensively investigated for its potential in environmental and energy applications owing to its high photoreactivity, non-toxicity, chemical stability, and low cost. However, its relatively large band gap of 3.2 eV limits its photocatalytic activity to the UV region, which accounts for

less than 5% of the solar spectrum. One effective strategy to enhance visible light absorption and improve charge separation efficiency is the formation of p–n heterojunctions by combining ZnO with other semiconductors of narrower band gaps. ZnO's versatility and tunable nanoscale morphology have made it an ideal material for optoelectronics, piezoelectric devices, nanosensors, and antibacterial surfaces. Its surface characteristics, defects, and crystallinity significantly influence its photocatalytic efficiency [7].

Cobalt oxide (Co_3O_4), a p-type semiconductor with a spinel structure, exhibits multiple oxidation states (Co^{2+}, Co^{3+}, and Co^{4+}), enabling a wide range of functional properties. Co_3O_4 nanoparticles possess direct band gaps around 1.48 eV and 2.19 eV and have been used in catalysis, gas sensors, energy storage systems, and low-temperature CO oxidation. Their multifunctional behavior arises from excellent optical, electrical, and magnetic properties [8].

Recent studies have highlighted the synergistic effects of ternary metal oxide nanocomposites in enhancing photocatalytic and antimicrobial properties. For example, Saadabasi et al. synthesized a ZnO–CeO_2–MgO composite using Ocimum basilicum L seed extract for biological and photocatalytic studies [9]. Similarly, Kannan et al. explored a CdO–CuO–ZnO nanocomposite synthesized via microwave irradiation, demonstrating notable antimicrobial and dye degradation performance [10]. Munawar et al. reported the antimicrobial activity of a NiO–CdO–ZnO nanocomposite prepared through homogeneous co-precipitation [4].

Several synthesis methods have been employed to fabricate such composites, including sol–gel [11], mechanical grinding [12], hydrothermal [13], microwave-assisted [14], solid-state reaction [15], and co-precipitation techniques [16]. Among these, the co-precipitation method stands out for its simplicity, cost-effectiveness, ambient synthesis conditions, and suitability for scaling [17].

In this study, we aim to investigate the structural, optical, and photocatalytic properties of a CdO–ZnO–Co_3O_4 ternary nanocomposite synthesized via co-precipitation. By optimizing the synthesis conditions and analyzing the resulting material, we explore its potential for use in photocatalytic wastewater treatment applications.

2. Experimental Procedure

2.1. Materials

The following analytical-grade reagents were used without further purification: cadmium nitrate tetrahydrate $Cd(NO_3)_2{\cdot}4H_2O$ (99%, HIMEDIA), zinc nitrate hexahydrate $Zn(NO_3)_2{\cdot}6H_2O$ (99%, HIMEDIA), cobalt nitrate hexahydrate $Co(NO_3)_2{\cdot}6H_2O$ (98%, HIMEDIA), sodium hydroxide NaOH (98%, HIMEDIA), and distilled water (DW).

2.2. Synthesis of CdO, ZnO, and Co_3O_4 Nanoparticles

To synthesize CdO nanoparticles, 0.03 M of $Cd(NO_3)_2{\cdot}4H_2O$ was dissolved in 100 mL of distilled water. A 0.1 M NaOH solution was added dropwise to the mixture until the pH reached 7, followed by stirring for one hour at room temperature. The resulting solution was stored overnight in a sealed container. The precipitate was then washed repeatedly with distilled water, dried at 100 °C for one hour, and ground using a mortar and pestle to obtain a fine powder. This powder was subsequently annealed at 500 °C for two hours to form CdO nanoparticles. The same procedure was repeated using $Zn(NO_3)_2{\cdot}6H_2O$ and $Co(NO_3)_2{\cdot}6H_2O$ to synthesize ZnO and Co_3O_4 nanoparticles, respectively.

2.3. Synthesis of CdO–ZnO–Co_3O_4 Nanocomposite

For the ternary nanocomposite, equal molar amounts (0.03 M each) of cadmium, zinc, and cobalt nitrates were dissolved in 300 mL of distilled water under continuous stirring for 10 minutes. The synthesis followed the same procedure described for the individual oxides. Before heat treatment, the resulting precipitate appeared blue, turning black after calcination. A schematic representation of the synthesis process is provided in Figure 1.

2.4. Characterization

X-ray diffraction (XRD) analysis was conducted using an XD-2 diffractometer (CuKα radiation, λ = 1.54 nm; 36 kV, 20 mA; China) at the Yemeni Geological Survey and Mineral Resources Board to determine the crystal structure. Elemental analysis was carried out using total reflection X-ray fluorescence (TXRF) spectroscopy (S8 TIGER, Bruker, Germany). The particle sizes and morphology of the synthesized samples were evaluated via transmission electron microscopy (TEM, JEM-2100, JEOL, Japan). Image analysis was performed using ImageJ software.

Optical properties were assessed using a UV-Vis-NIR spectrophotometer (Cary 5000, Model DRA-2500, JASCO V-750, Japan) in the 400–700 nm wavelength range to obtain diffuse reflectance spectra (DRS). Photocatalytic activity was studied using a UV-VISIBLE spectrophotometer (UV-1650 PC, SHIMADZU, Japan) covering the 190–1100 nm range, conducted at the Department of Chemistry, Faculty of Science, Suez Canal University.

2.5. Photocatalytic activity

The photocatalytic efficiency of the synthesized samples was evaluated by degrading methylene red (MR) dye under UV irradiation. In a typical test, 20 mg of each nanoparticle (CdO, ZnO, Co_3O_4, and the ternary nanocomposite) was added to 100 mL of a 10 ppm MR aqueous solution in a beaker. MR dye was selected due to its effective coloring properties, relative environmental safety, and high biodegradability, making it a more sustainable alternative to conventional dyes.

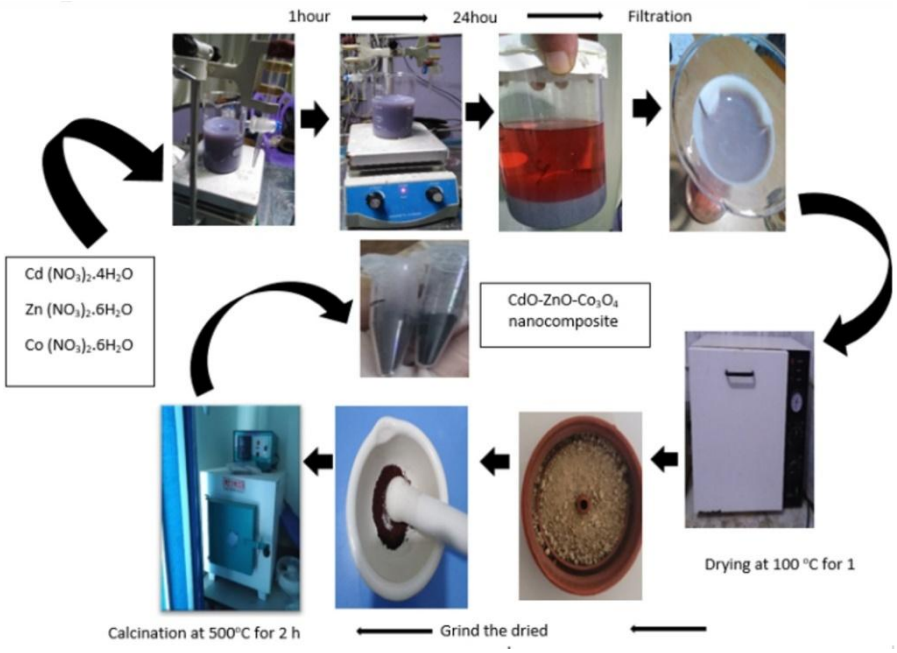

Figure 1: Schematic illustration of the CdO–ZnO–Co_3O_4 nanocomposite synthesis procedure.

The suspension was stirred magnetically in a custom-built photocatalytic reactor for two hours to establish adsorption–desorption equilibrium. A 320-watt UV lamp positioned 30 cm above the solution was then used to initiate photocatalysis. Aliquots of 5 mL were collected at 30-minute intervals, centrifuged, and analyzed via UV-Vis spectrophotometry to monitor the decrease in dye concentration through absorbance measurements.

3. Results and Discussion

3.1 Structural Analysis

The XRD patterns of CdO, ZnO, Co_3O_4 nanoparticles, and their CdO–ZnO–Co_3O_4 nanocomposite were recorded in the 2θ range of 30°–80° (Fig. 2). The diffraction peaks are indicative of distinct crystal planes. Peaks at 33.4°, 38.8°, 55.8°, 66.3°, and 69.7° correspond to (111), (200), (220), (311), and (222) planes, respectively, and match the JCPDS card #01-1049, confirming the cubic structure of CdO [5,18]. For ZnO, peaks at 32.5°, 34.8°, 36.7°, 48°, 57°, 63.3°, 66.6°, 68.4°, 69.5°, and 73° align with (100), (002), (101), (102), (110), (103), (200), (112), (201), and (004) planes per JCPDS card #01-1136, confirming a hexagonal structure [17,19]. Co_3O_4 shows peaks at 31.6°, 37.2°, 38.8°, 45.2°, 59.7°, and 65.6°, which correspond to (220), (311), (222), (400), (511), and (440) planes, confirming a cubic spinel structure consistent with JCPDS card #042-1467 [1].

In the nanocomposite, ZnO exhibited the most intense peaks, while CdO showed the weakest, suggesting that Co_3O_4's low crystallinity notably influenced the overall structural integrity. The crystallite sizes (D) were calculated using the Scherrer equation [20]:

$$D = \frac{0.9\lambda}{\beta \cos\theta} \quad (1)$$

where λ is the X-ray wavelength, β is the full width at half maximum in radians, and θ is the Bragg angle.

Lattice constants for cubic and hexagonal systems, respectively, were determined using Bragg's law [21]:

$$\frac{1}{d^2} = \frac{h^2 + k^2 + l^2}{a^2} \quad (2)$$

$$\frac{1}{d^2} = \frac{4}{3}\left[\frac{h^2 + hk + k^2}{a^2}\right] + \frac{l^2}{c^2} \quad (3)$$

Unit cell volumes were calculated as [22, 23]:

$$V = a^3 \quad \textbf{(cubic)} \quad (4)$$

$$V = 0.866\, a^2 c \quad \textbf{(hexagonal)} \quad (5)$$

Microstrain (ε) and dislocation density (δ) were estimated as [24]:

$$\varepsilon = \frac{\beta}{4 \tan\theta} \quad (6)$$

$$\delta = \frac{1}{D^2} \quad (7)$$

Results are summarized in Table 1. The nanocomposite exhibited a pronounced decrease in crystallite size, attributed to an increase in dislocation density and strain. This reduction is attributed to greater nucleation sites, interfacial disruptions, and impurity incorporation, which hinder grain growth and stabilize smaller crystalline domains [1].

Table 1: Structural parameters of CdO, ZnO, Co_3O_4 NPs, and CdO–ZnO–Co_3O_4 nanocomposite.

Samples	D (nm)	a (Å)	c (Å)	V (Å^3)	ε ($\times10^{-3}$)	δ ($\times10^{-3}$) (Lines/nm^2)
CdO NPs	37.73	4.64	–	99.9	1.6	0.702
ZnO NPs	31.79	3.20	5.14	45.5	3.9	0.989
Co_3O_4 NPs	32.84	8.13	–	537.3	6.4	0.927
CdO-ZnO-Co_3O_4 Nanocomposite						
CdO	26.25	4.63	–	99.25	4.7	1.541
ZnO	14.27	3.20	5.15	45.67	8.8	4.790
Co_3O_4	13.45	8.06	–	523.6	15.5	5.527

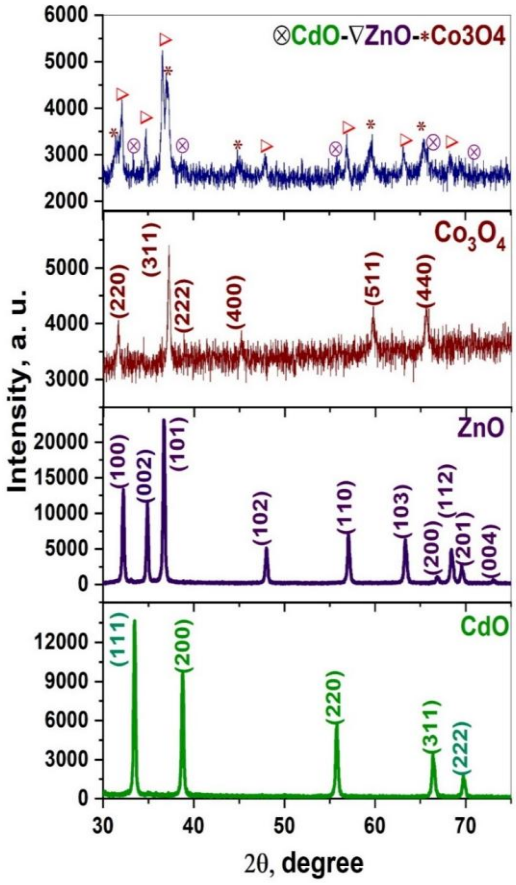

Figure 2: XRD patterns of CdO, ZnO, Co_3O_4 nanoparticles and CdO–ZnO-Co_3O_4 nanocomposite.

3.2. Elemental Analysis

TXRF analysis confirmed the elemental composition of the CdO–ZnO–Co_3O_4 nanocomposite. Results are summarized in Table 2. The percentages align closely with the intended stoichiometry, indicating successful incorporation of all three metal oxides.

Table 2: TXRF elemental analysis of CdO–ZnO–Co_3O_4 nanocomposite.

Element	% Metal	Compound	% Compound
Cd	18.79	CdO	23.8
Zn	38.66	ZnO	48.42
Co	21.35	Co_3O_4	27.2
O_2	20.62	–	–
Impurities: (P, Si, S, Ca, Fe)	0.58	–	0.58
Total	**100**	**–**	**100**

3.3. TEM Analysis

Figure 3 shows TEM images for CdO, ZnO, Co_3O_4 nanoparticles, and the ternary nanocomposite. Spherical to semi-spherical particles were observed across all samples. Using ImageJ, average particle sizes were calculated: CdO (60.8 nm), ZnO (51.8 nm), Co_3O_4 (33.3 nm), and nanocomposite (13.8 nm).

Transmission electron microscope (TEM) images, as shown in Figure 3, display CdO, ZnO, and Co_3O_4 nanoparticles, as well as a CdO–ZnO–Co_3O_4 nanocomposite. The TEM images show nanoparticles of varied shapes and sizes. The TEM images of the samples in Figure 3 clearly show the spherical and semispherical shapes of the prepared nanoparticles. Their particle sizes were determined using the ImageJ program. The histogram is plotted in Figure 4. The CdO–ZnO–Co_3O_4 nanocomposite and CdO, ZnO, and Co_3O_4 nanoparticles have particle sizes of 13.8 nm, 60.8 nm, 51.8 nm, and 33.3 nm, respectively. The comparison selected area electron diffraction (SAED) pattern for CdO, ZnO, and Co_3O_4 nanoparticles, as well as the CdO–ZnO–Co_3O_4 nanocomposite, is shown in Figure 5. The planes

corresponding to different rings were found by using the ImageJ program to calculate the d-spacing, which agrees well with the results of TXRF and XRD. The circular fringes in SAED patterns indicate the polycrystalline nature of the samples, and the diffraction rings matched with the XRD d-spacing of CdO, ZnO, Co_3O_4 nanoparticles, and CdO–ZnO–Co_3O_4 nanocomposite. This outcome aligns with that of Aziz *et al.* [17].

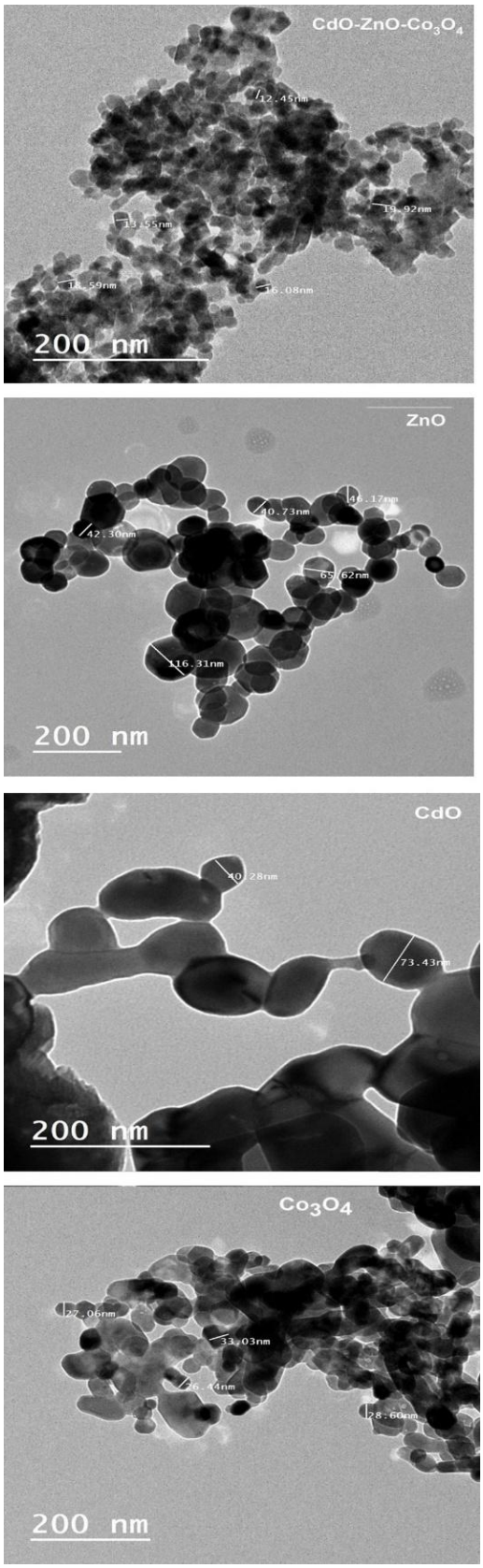

Figure 3: TEM image of CdO, ZnO, and Co_3O_4 nanoparticles and CdO–ZnO–Co_3O_4 nanocomposite.

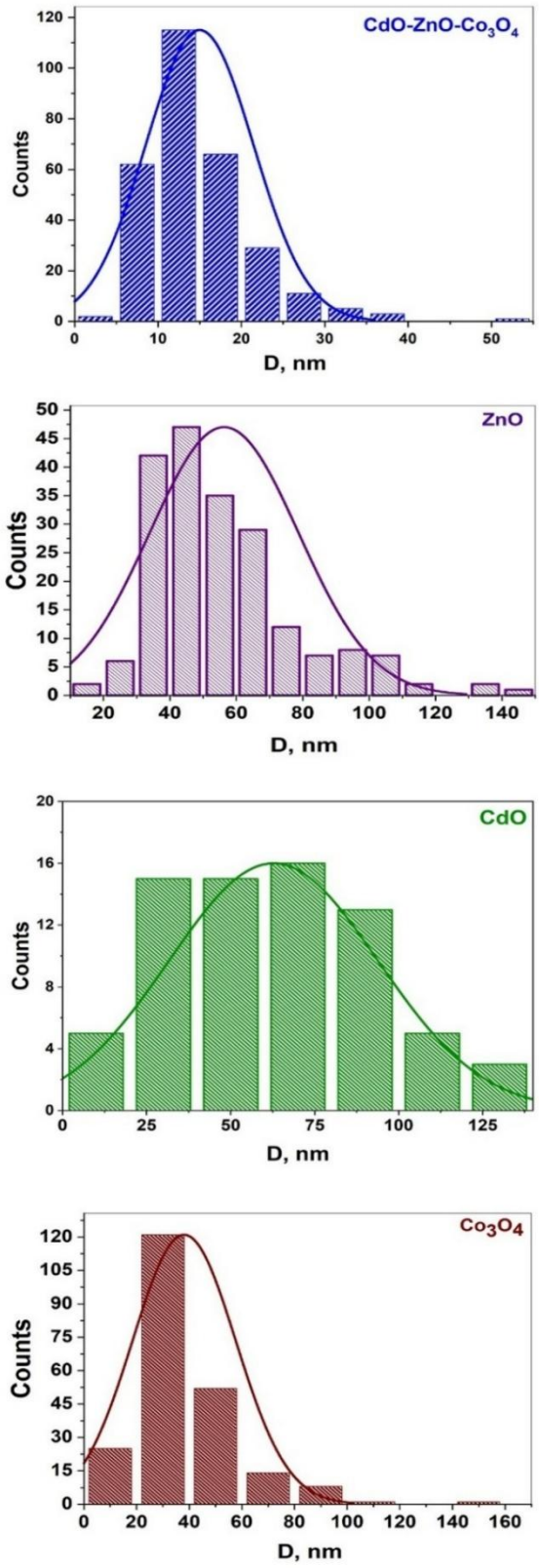

Figure 4: Histograms calculated from TEM images for the of CdO, ZnO, and Co_3O_4 nanoparticles and CdO–ZnO–Co_3O_4 nanocomposite

3.4. Optical Properties

Diffuse reflectance spectra (Figure 6) revealed differences in reflectance across the samples, with CdO and the nanocomposite exhibiting higher reflectance than ZnO and Co_3O_4. For the CdO–ZnO–Co_3O_4 nanocomposite, the onset of reflectance occurred around 400 nm, within the visible range.

The optical band gap (E_g) was estimated using the Kubelka-Munk function [25, 26]:

$$F(R_\infty) = \frac{(1 - R_\infty)^2}{2R_\infty} \quad (8)$$

where $F(R_\infty)$ is called the remission or Kubelka–Munk function and the diffuse reflectance (R_∞) of the examined samples $R_\infty = R_{sample}/R_{standard}$ [27]. Band gap values were determined from Tauc plots using:

$$(F(R_\infty) \times hv)^2 = A(hv - E_g) \quad (9)$$

The values of the optical band gap (E_g) are obtained by plotting the variation of $(F(R_\infty) \times hv)^2$ versus E (or hv) and extending the straight-line range of these plots on the E axis and the obtained. Values are shown in Table 3.

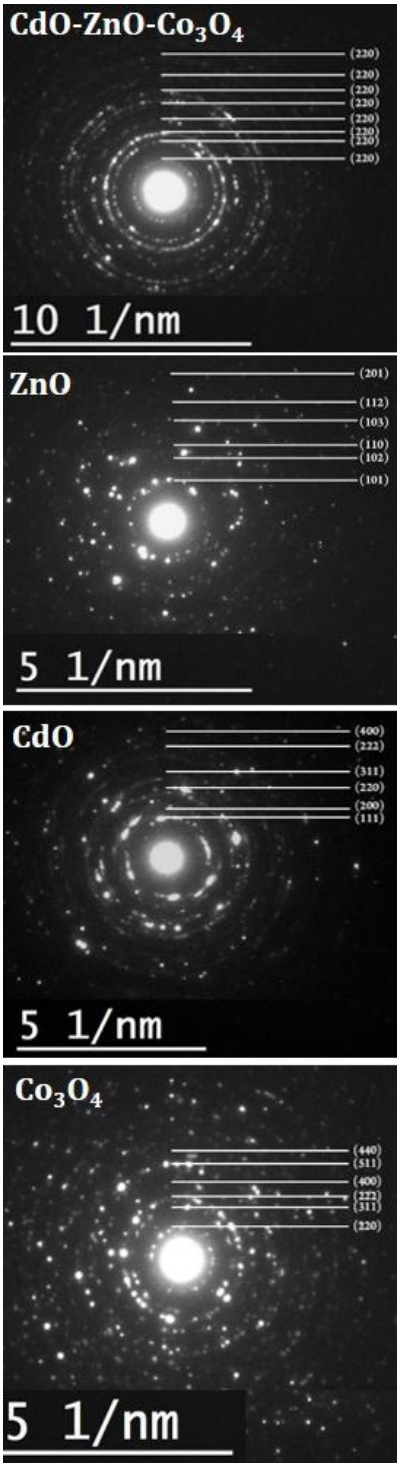

Figure 5: SAED patterns of CdO, ZnO, and Co_3O_4 nanoparticles and CdO–ZnO–Co_3O_4 nanocomposite.

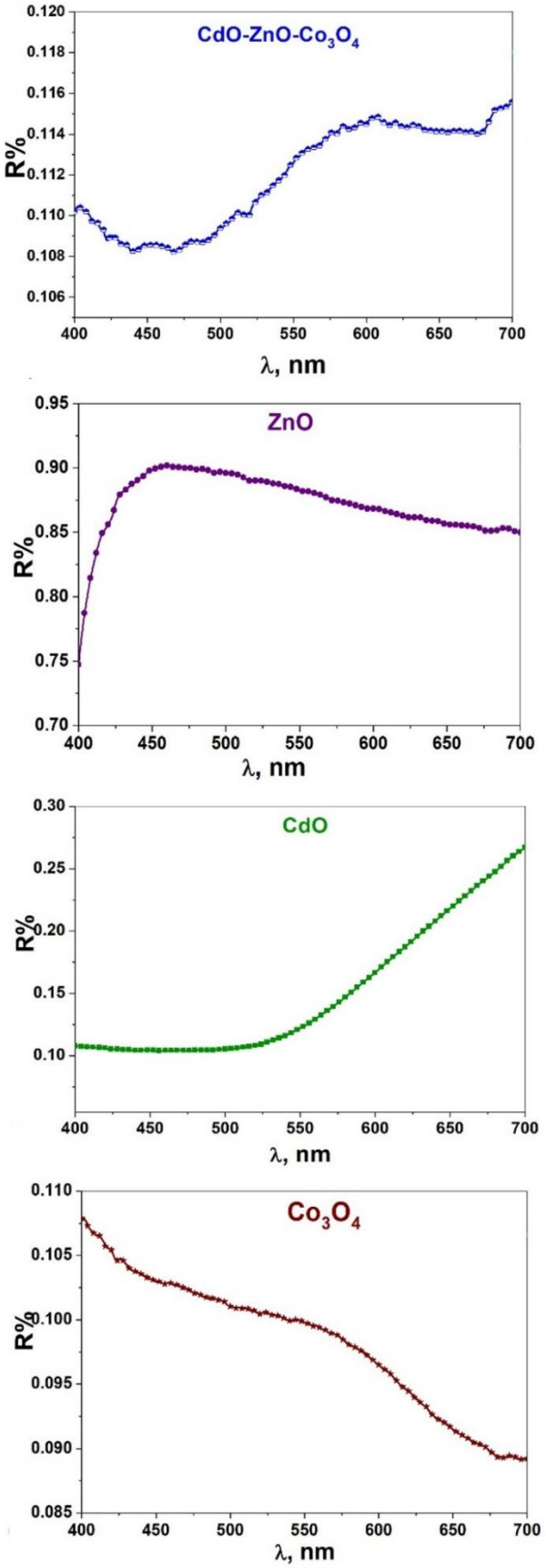

Figure 6: Diffuse reflectance spectrum (R%) of the CdO, ZnO, and Co_3O_4 nanoparticals and CdO–ZnO–Co_3O_4 nanocomposite

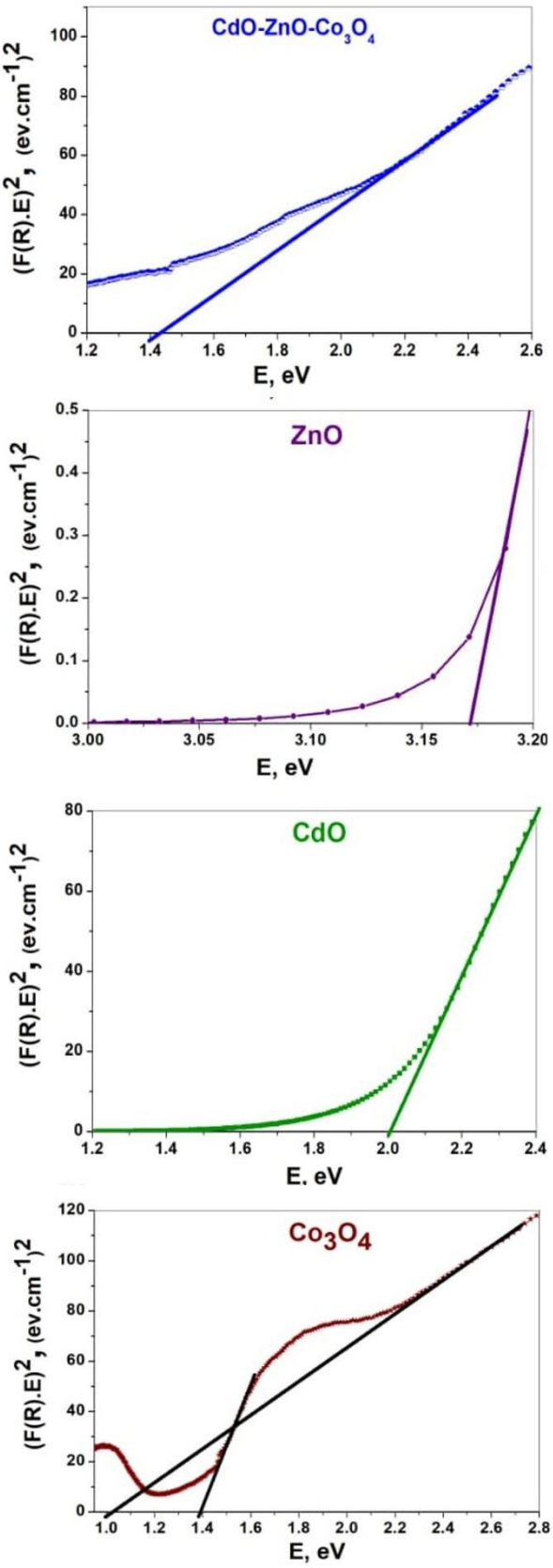

Figure 7: The plot of $(F(R)\hbar\nu)^2$ vs $E(eV)$ for the direct band gap energy for the prepared samples.

As shown in Figure 7 and Table 3, the optical band gap of CdO NPs was 2 eV, corresponding to the direct transition from the valence band O **2p** states to the shallow cores of **d** states of **4d** for Cd [28, 29]. ZnO NPs explored an optical band gap value of 3.17 eV, which is attributed to the transitions from the filled valence O **2p** orbitals to the empty conduction Zn **4s** orbitals, with the possibility of some Zn **4p** orbitals [25, 30]. For the Co_3O_4 NPs, Co^{2+} and Co^{3+} ions contribute to their electrical characteristics. Different charge transfer processes can be attributed to the two band gap energy values (E_{g1} and E_{g2}). The first one (E_{g1}), which is 1 eV, is associated with the charge transfer transition from O^{2-} ions to Co^{3+} ions. The excitation of electrons from the valence band to a higher energy state associated with Co^{3+} makes this transition significant. The second value (E_{g2}), approximately 1.43 eV, is associated with the change in ions from O^{2-} to Co^{2+}, suggesting that, unlike the Co^{3+} transition, the lower energy transition involves a distinct electronic configuration and energy state.

Table 3: Optical band gap energy values of CdO, ZnO, Co_3O_4 nanoparticles, and CdO–ZnO–Co_3O_4 nanocomposite.

Sample	E_g (eV)
CdO	2.00
ZnO	3.17
Co_3O_4	1.00, 1.43
CdO-ZnO-Co_3O_4	1.40

Although it is coupled to crystal size, it is not always directly correlated with the band gap, which suggests that for certain materials, other factors, such as surface states or structural integrity, may have a more significant or negligible impact on the effects of particle size on optical characteristics [31]. The CdO–ZnO–Co_3O_4 nanocomposite has a band gap value close to the second optical band gap of the Co_3O_4 NPs, which was 1.4 eV. This result may be related to the fact that the Co_3O_4 oxide is the dominant oxide in the nanocomposite. Besides the optical band gap of the nanocomposite, which is equal to that of Co_3O_4, the crystallinity of the nanocomposite is as weak as that of Co_3O_4.

On the other hand, ZnO oxide has the highest percentage, as determined by TXRF measurements, and it also exhibits the highest peak intensity in the X-ray pattern of the nanocomposite. These two results may be related to the preparation conditions that led to the formation of ZnO in the nanocomposite with a higher content than other oxides. Therefore, the dominant oxide in the nanocomposite is Co_3O_4 and not ZnO. At the interfaces of several metal oxides, new energy states may form, which could explain the shift in the band gap (E_g) of the nanocomposite relative to that of the individual metal oxides.

Photocatalytic activity is increased when the energy gap is reduced. Photocatalysts with narrow band gap values can absorb a broader range of visible light, which is important because the majority of solar radiation falls within the visible spectrum, and photocatalytic activity is directly correlated with efficient light absorption [1].

3.5. Photocatalytic Activities

3.5.1. Photocatalytic Mechanism

The photocatalytic mechanism of the CdO–ZnO–Co_3O_4 nanocomposite under UV light irradiation is illustrated in Figure 8. Upon exposure to UV photons with energy equal to or greater than the bandgap of the nanocomposite, electrons (e^-) in the valence band (VB) of each component semiconductor (CdO, ZnO, Co_3O_4) are excited to their respective conduction bands (CB), leaving behind positively charged holes (h^+) in the VB. The charge separation and subsequent migration are facilitated by the formation of heterojunctions between the n-type (CdO and ZnO) and p-type (Co_3O_4) semiconductors.

In this ternary system, ZnO with its higher conduction band edge serves as an electron donor to CdO and Co_3O_4, while Co_3O_4 effectively accepts holes due to its suitable VB position. This directional movement of photogenerated charge carriers minimizes recombination rates and enhances photocatalytic activity.

The photogenerated holes (h^+) react with water molecules or surface hydroxyl groups to form hydroxyl radicals (•OH), which are highly oxidative. Simultaneously, conduction band electrons reduce adsorbed molecular oxygen (O_2) to generate superoxide radicals ($O_2^{\bullet-}$). These radicals further interact to form additional reactive oxygen species (ROS) such as hydrogen peroxide (H_2O_2) and more hydroxyl radicals, significantly contributing to the degradation of organic pollutants like

methylene red (MR). The comprehensive mechanism includes the following reactions [32]:

$$CdO–ZnO–Co_3O_4 + h\nu \rightarrow e^- + h^+ \quad (10)$$

$$h^+ + H_2O \rightarrow \bullet OH + H^+ \quad (11)$$

$$e^- + O_2 \rightarrow O_2\bullet^- \quad (12)$$

$$O_2\bullet^- + H^+ \rightarrow \bullet HO_2 \rightarrow H_2O_2 \rightarrow \bullet OH \quad (13)$$

$$\bullet OH + \text{dye (MR)} \rightarrow \text{degradation products} \quad (14)$$

This synergistic interaction among the three oxides enhances the generation of active radicals, thereby improving the overall photocatalytic performance of the nanocomposite.

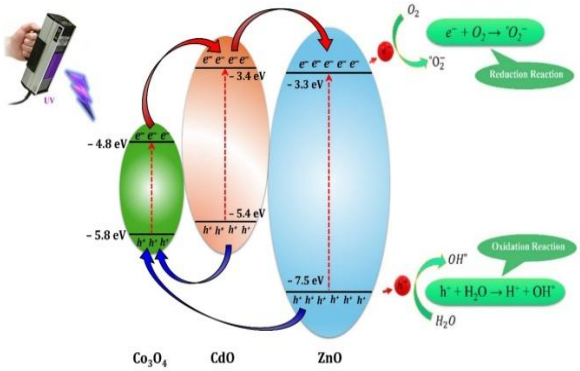

Figure 8: The mechanism of the photocatalytic process for the CdO–ZnO–Co_3O_4 nanocomposite under UV irradiation.

3.5.2. Photodegradation and Catalyst Concentration Effect

The photodegradation behavior of MR dye under UV irradiation at 320 nm in the presence of the CdO–ZnO–Co_3O_4 nanocomposite catalyst was assessed over varying time intervals. As depicted in Figure 9, the absorbance of the MR solution gradually decreased, indicating progressive degradation of the dye. The maximum absorption peak at 419.8 nm, characteristic of MR, diminished significantly after 30 minutes of exposure.

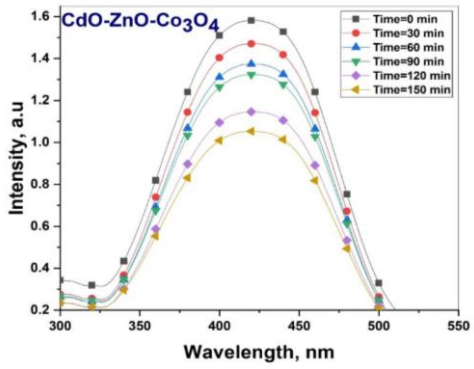

Figure 9: Absorbance spectrum of the CdO- ZnO-Co_3O_4 nanocomposite for MR dye under UV irradiation.

The degradation efficiency was quantified using the relation [33]:

$$\textit{Degradation}\ \% = \left[\frac{(A_o - A_t)}{A_o}\right] \times 100 \quad (15)$$

where A_o is the initial absorbance (at time zero) and A_t represents absorbance after a particular time. The data revealed a degradation efficiency of approximately 33.4% within 30 minutes (Figure 10A). This modest degradation rate may be attributed to factors such as limited active site availability, suboptimal light penetration due to the MR concentration, and recombination of charge carriers. Several factors, including catalyst concentration, influence the observed photocatalytic performance. At optimal concentrations, more active sites are available for photon absorption and redox reactions. However, excessive catalyst loading can lead to light scattering and shielding effects, which reduce photon penetration and the overall reaction rate. Because light shielding effects caused by higher pollutant concentrations can result in reduced efficiency, as not all dye molecules are exposed to the light required for degradation [34]. The present photocatalytic degradation efficiency is compared with some metal oxide nanocomposites (Table 4).

Table 4: Comparison of photocatalytic activity of some metal oxide nanocomposites

Sample	Dye*	Light Source	Efficiency	Time (min)	Ref.
CeO_2/PAM	MB	UV	65%	15	[35]
CeO_2/GO/PAM	MB	UV	53%	15	[35]
CeO_2/GO/PAM/AO	MB	UV	49%	15	[35]
CeO_2/GO/PAM/$AgNO_3$	MB	UV	46%	15	[35]
ZnO/CeO_2 (99:01)	MO	Visible light	39.5%	30	[36]
ZnO/CeO_2(99:01)	MB	Visible light	34.7%	30	[36]
ZnO/CeO_2(99:01)	Phenol	Visible light	33.5%	30	[36]
CdO–NiO	RhB	UV	78%	20	[37]
CdO–ZnO–Co_3O_4	MR	UV	33.4%	30	This study

MB: Methyl Blue, MO: Methyl Orange, RhB: Rhodamine B, and MR: Methyl Red.

Reaction kinetic models can be used to explain the time-dependent relationship between system operating parameters and the rate at which organic pollutants degrade or microorganisms become inactive. We can use the following relationship [1] to calculate pseudo-first-order kinetics.

$$\ln\left(\frac{C_t}{C_0}\right) = Kt \quad (16)$$

where C_o is the concentration before light irradiation, C_t is the concentration at the time, and K is a first-order constant. When $ln\ (\frac{C_0}{C_t})$ is plotted against time, t (Figure 10B), the slope of the straight-line segment yields the value of K. A linear relationship was observed when plotting $ln\ (\frac{C_0}{C_t})$ versus time (Fig. 10b), with the rate constant K calculated as 0.00271 min^{-1}. This value suggests a relatively slow degradation rate under the tested conditions, which could be improved through modifications such as increased catalyst loading, optimized dye concentration, or adjusting the light intensity.

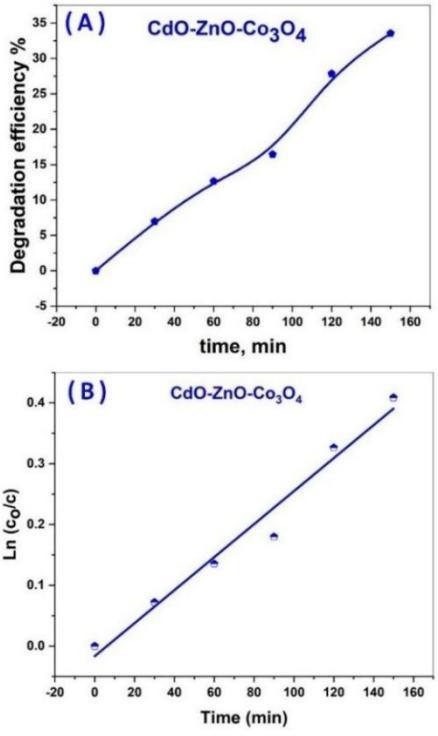

Figure 10: (A) MR degradation%, (B) Photodegradation kinetics plots of MR.

When compared with other nanocomposite systems (as shown in Table 4), the current photocatalyst demonstrates moderate activity. However, its ease of synthesis, structural stability, and reduced band gap energy highlight its potential for further development and application in wastewater treatment.

4. Conclusion

In this study, CdO, ZnO, and Co_3O_4 nanoparticles, along with their mixed ternary oxide nanocomposite CdO–ZnO–Co_3O_4, were successfully synthesized via the co-precipitation method. XRD analysis revealed a significant reduction in crystallite size for the nanocomposite compared to the individual nanoparticles, indicating effective integration of the phases. The elemental composition, as confirmed by TXRF analysis, aligned with the structural phases observed in XRD. TEM imaging showed uniformly distributed spherical particles, while SAED patterns validated the polycrystalline nature of the samples. Optical characterization using diffuse reflectance spectroscopy revealed that the nanocomposite exhibited a reduced band gap of 1.4 eV, enhancing its ability to harness UV light. Photocatalytic performance testing against methylene red dye demonstrated a degradation efficiency of 33.5% within 30 minutes of UV exposure, affirming the potential of CdO–ZnO–Co_3O_4 as a promising UV-active photocatalyst for wastewater treatment applications.

Data Availability

The datasets used and analyzed during the current study are available from the corresponding author upon reasonable request.

Conflict of Interest

The authors declare that there are no conflicts of interest regarding the publication of this study.

Funding

This research received no external funding.

Acknowledgment

The authors gratefully acknowledge Thamar University, Genius University for Sciences & Technology (Yemen), and Suez Canal University (Egypt) for their technical support throughout this study.

References

[1] Singh, R.P., Singh, P., Singh, K.R.,(2021) Introduction to Composite Materials: Nanocomposites and Their Potential Applications, in: Sachdeva, A., Singh, P.K., Rhee, H.W., (Ed.), Composite Materials, *CRC Press*, Boca Raton, USA, pp. 1-28.

[2] Weldegebrieal, G.K., Hinsene, D.H., and Sibhatu, A.K. (2023) Photocatalytic activity of CdO/ZnO nanocomposite for methylene blue dye and parameters optimisation using response surface methodology, *International Journal of Environmental Analytical Chemistry* **103**: 6146-6168.

[3] Guo, T., Yao, M.-S., Lin, Y.-H., Nan, C.-W. (2015) A comprehensive review on synthesis methods for transition-metal oxide nanostructures, *CrystEngComm* **17**: 3551-3585.

[4] Munawar, T., Iqbal, F., Yasmeen, S., Mahmood, K., Hussain, A. (2020) Multi metal oxide NiO-CdO-ZnO nanocomposite–synthesis, structural, optical, electrical properties and enhanced sunlight driven photocatalytic activity, *Ceramics International* **46**: 2421-2437.

[5] Aziz, S.N., Abdulwahab, A., Aldeen, T.S. (2024) Synthesis and Characterization of (CdO-CuO-Co_3O_4) Mixed Metal Oxides Nanocomposite, *Sana'a University Journal of Applied Sciences and Technology* **2**: 116-123.

[6] Taufik, A., Tju, H., Prakoso, S.P., Saleh, R. (2018) Different routes of synthesized CdO nanoparticles through microwave-assisted methods and photocatalytic study, *AIP Conference Proceedings* **2023**: 020035-1-020035-5.

[7] Chimupala, Y., Phromma, C., Yimklan, S., Semakul, N., Ruankham, P. (2020) Dye wastewater treatment enabled by piezo-enhanced photocatalysis of single-component ZnO nanoparticles, *RSC Advances* **10**: 28567-28575.

[8] Vennela, A.B., Mangalaraj, D., Muthukumarasamy, N., Agilan, S., Hemalatha, K.V. (2019) Structural and Optical Properties of Co_3O_4 Nanoparticles Prepared by Sol-gel Technique for Photocatalytic Application, *International Journal of Electrochemical Science* **14**: 3535-3552.

[9] Saadabadi, R.H., Tehrani, F.S., Darroudi, M., Sabouri, Z. (2024) Plant-based synthesis of ZnO–CeO_2–MgO nanocomposite using *Ocimum Basilicum* L seed extract: Biological effects and photocatalytic activity, *Materials Chemistry and Physics* **314**: 128919.

[10] Kannan, K., Radhika, D., Gnanasangeetha, D., Lakkaboyana, S.K., Sadasivuni, K.K., Gurushankar, K., Hanafiah, M.M. (2021) Photocatalytic and antimicrobial properties of microwave synthesized mixed metal oxide nanocomposite, *Inorganic Chemistry Communications* **125**: 108429.

[11] Singh, L.P., Bhattacharyya, S.K., Kumar, R., Mishra, G., Sharma, U., Singh, G., Ahalawat, S. (2014) Sol-Gel processing of silica nanoparticles and their applications, *Advances in Colloid and Interface Science* **214**: 17-37.

[12] Yamanaka, S., Suzuma, A., Fujimoto, T., Kuga, Y. (2013) Production of scallop shell nanoparticles by mechanical grinding as a formaldehyde adsorbent, *Journal of Nanoparticle Research* **15**: 1573.

[13] Li, J., Wu, Q., Wu, J.,(2016) Synthesis of nanoparticles via solvothermal and hydrothermal methods, in: Aliofkhazraei, M., (Ed.), Handbook of Nanoparticles, *Springer international publishing Switzerland*, Cham, Switzerland, pp. 295-328.

[14] Hasanpoor, M., Aliofkhazraei, M., Delavari, H. (2015) Microwave-assisted Synthesis of Zinc Oxide Nanoparticles, *Procedia Materials Science* **11**: 320-325.

[15] Zhu, Y., Zhou, Y. (2008) Preparation of pure ZnO nanoparticles by a simple solid-state reaction method, *Applied Physics A* **92**: 275-278.

[16] Vaidyanathan, G., Sendhilnathan, S., Arulmurugan, R. (2007) Structural and magnetic properties of $Co_{1-x}Zn_xFe_2O_4$ nanoparticles by co-precipitation method, *Journal of Magnetism and Magnetic Materials* **313**: 293-299.

[17] Aziz, S.N., Abdulwahab, A.M., Aldeen, T.S., Alqabili, D.M.A. (2024) Synthesis, characterization, and evaluation of antibacterial and antifungal activities of CuO-ZnO-Co_3O_4 nanocomposites, *Heliyon* **10**: e37802.

[18] Hedayati, K. (2023) Synthesis, characterization and photocatalytic properties investigation of $CuFe_2O_4$/CdO nanocomposite, *Nano Science and Technology Journal* **1**: 49-55.

[19] Dhal, J.P., Mishra, B.G., Hota, G. (2015) Hydrothermal synthesis and enhanced photocatalytic activity of ternary Fe_2O_3/$ZnFe_2O_4$/ZnO nanocomposite through cascade electron transfer, *RSC Advances* **5**: 58072-58083.

[20] Abdulwahab, A.M., Al-Adhreai, A.a.A., Ahmed, A.A.A. (2021) Influence of Ni-Co dual doping on structural and optical properties of CdSe thin films prepared by chemical bath deposition method, *Optik* **236**: 166659.

[21] Othman, A.A., Al-Hammadi, A., Khoreem, S.H. (2023) Fabrication and Study of the Effect of Mn-Substituted Ba-Zn Nanoferrites on the Enrichment of Structural Properties, *Sana'a University Journal of Applied Sciences and Technology* **1**: 168-74.

[22] Al-Sharabi, A., Sada'a, K.S.S., Al-Osta, A., Abd-Shukor, R. (2022) Structure, optical properties and antimicrobial activities of MgO–$Bi_{2-x}Cr_xO_3$ nanocomposites prepared via solvent-deficient method, *Scientific Reports* **12**: 10647.

[23] Yathisha, R.O., Nayaka, Y.A., Vidyasagar, C.C. (2016) Microwave combustion synthesis of hexagonal prism shaped ZnO nanoparticles and effect of Cr on structural, optical and electrical properties of ZnO nanoparticles, *Materials Chemistry and Physics* **181**: 167-175.

[24] Al-Mushki, A.A.A., Ahmed, A.A.A., Abdulwahab, A.M., Qaid, S.A.S., Alzayed, N.S., Shahabuddin, M., Abduljalil, J.M.A., Saad, F.A.A. (2023) Effect of the molar ratio of (Ni^{2+} and Fe^{3+}) on the magnetic, optical and antibacterial properties of ternary metal oxide CdO–NiO–Fe_2O_3 nanocomposites, *Scientific Reports* **13**: 9021.

[25] Ahmed, A.A.A., Talib, Z.A., Hussein, M.Z.b., Zakaria, A. (2012) Improvement of the crystallinity and photocatalytic property of zinc oxide as calcination product of Zn–Al layered double hydroxide, *Journal of Alloys and Compounds* **539**: 154-160.

[26] Ahmed, A.A.A., Talib, Z.A., Hussein, M.Z. (2015) Influence of sodium dodecyl sulfate concentration on the photocatalytic activity and dielectric properties of intercalated sodium dodecyl sulfate into Zn–Cd–Al layered double hydroxide, *Materials Research Bulletin* **62**: 122-131.

[27] Torrent, J., Barrón, V.,(2002) Diffuse reflectance spectroscopy of iron oxides, in: Hubbard, A.T., (Ed.), Encyclopedia of surface and Colloid Science, *Marcel Dekker, Inc.*, New York, USA, pp. 1438-1446.

[28] Guerrero-Moreno, R.J., Takeuchi, N. (2002) First principles calculations of the ground-state properties and structural phase transformation in CdO, *Physical Review B* **66**: 205205.

[29] Lims, S.C., Jose, M., Aswathappa, S., Dhas, S.S.J., Kumar, R.S., Pham, P.V. (2024) Co-precipitation synthesis of highly pure and Mg-doped CdO nanoparticles: from rod to sphere shapes, *RSC Advances* **14**: 22690-22700.

[30] Sampath, S.K., Cordaro, J.F. (1998) Optical Properties of Zinc Aluminate, Zinc Gallate, and Zinc Aluminogallate Spinels, *Journal of the American Ceramic Society* **81**: 649-654.

[31] Andrade, A.B., Ferreira, N.S., Valerio, M.E.G. (2017) Particle size effects on structural and optical properties of BaF_2 nanoparticles, *RSC Advances* **7**: 26839-26848.

[32] Akyüz, D. (2021) rGO-TiO_2-CdO-ZnO-Ag photocatalyst for enhancing photocatalytic degradation of methylene blue, *Optical Materials* **116**: 111090.

[33] Shinde, R.S., Khairnar, S.D., Patil, M.R., Adole, V.A., Koli, P.B., Deshmane, V.V., Halwar, D.K., Shinde, R.A., Pawar, T.B., Jagdale, B.S., Patil, A.V. (2022) Synthesis and Characterization of ZnO/CuO Nanocomposites as an Effective Photocatalyst and Gas Sensor for Environmental Remediation, *Journal of Inorganic and Organometallic Polymers and Materials* **32**: 1045-1066.

[34] Hassanpour, M., Safardoust-Hojaghan, H., Salavati-Niasari, M. (2017) Degradation of methylene blue and Rhodamine B as water pollutants via green synthesized Co_3O_4/ZnO nanocomposite, *Journal of Molecular Liquids* **229**: 293-299.

[35] Kalaycıoğlu, Z., Özuğur Uysal, B., Pekcan, Ö., Erim, F.B. (2023) Efficient Photocatalytic Degradation of Methylene Blue Dye from Aqueous Solution with Cerium Oxide Nanoparticles and Graphene Oxide-Doped Polyacrylamide, *ACS Omega* **8**: 13004-13015.

[36] Rajendran, S., Khan, M.M., Gracia, F., Qin, J., Gupta, V.K., Arumainathan, S. (2016) Ce^{3+}-ion-induced visible-light photocatalytic degradation and electrochemical activity of ZnO/CeO_2 nanocomposite, *Scientific Reports* **6**: 31641.

[37] Linda, T., Muthupoongodi, S., Shajan, X.S., Balakumar, S. (2016) Fabrication and characterization of chitosan templated CdO/NiO nano composite for dye degradation, *Optik* **127**: 8287-8293.